A method to predict energy barriers in stress modulated solid–solid phase transitions

Arman Ghasemi, Wei Gao*

Department of Mechanical Engineering, University of Texas at San Antonio, Texas, San Antonio, TX 78249, USA

ARTICLE INFO

ABSTRACT

Stress can be applied to modulate solid–solid phase transitions because the stress changes the transition energy barrier which determines the phase transition rate. The lower the barrier, the higher the rate and more likely the phase transition occurs. This paper presents a new theoretical method – *finite deformation Bell theory* (FD-BT), which is developed based on the concept of the original Bell theory, for predicting transition barriers as a function of the applied stress field. The theory is applied to study the phase transitions of two model materials which exhibit distinct transition mechanisms: 2D MoTe$_2$ from 2H phase to 1T′ phase, and silicon from diamond phase to β-tin phase. The theoretical predictions are compared with the atomistic simulation results obtained from the *finite deformation nudged elastic band* (FD-NEB) method, which has been recently developed to compute stress dependent barriers of the transitions under finite deformation.

© 2019 Elsevier Ltd. All rights reserved.

1. Introduction

Solid–solid phase transition has been an important topic in mechanics and materials research as it appears on many material systems. The dynamic control of transitions between different phases can lead to broad technological applications. Particularity, stress can be directly employed as a useful tool to control phase transition process. Meanwhile, stress also commonly exists and plays important role in various phase engineering techniques.

The fundamental mechanism of stress modulated phase transition can be described by Fig. 1, in which a material transfers from a stable phase P1 to another stable phase P2. The most probable phase transition path, i.e. *minimum energy path* (MEP), is illustrated by a double-well curve. To have a phase transition from P1 to P2, the material has to overcome a barrier ($\Pi^{\neq}$) by crossing the transition state at the peak of MEP. Based on the transition state theory within the harmonic approximation (Hanggi et al., 1990; Olsen, 2006), the barrier determines the phase transition rate (through an exponential function shown in the figure, see detailed discussion in Section 2.2), which is an important thermodynamic variable that determines the likelihood of phase transition. The lower the barrier, the higher the rate and more likely the transition occurs. The MEP can be modulated by the applied stress field. Under an external stress, the energy landscape is generalized to a static enthalpy landscape (not including kinetic energy) in order to include the work done by external stresses. In Fig. 1, the stress $\mathbf{S}_1$ reduces the barrier between phase P1 and the transition state, thereby facilitating the transition from P1 to P2. By contrast, the stress $\mathbf{S}_2$ raises this barrier so prohibits the transition from P1 to P2; meanwhile it lowers the barrier

* Corresponding author.
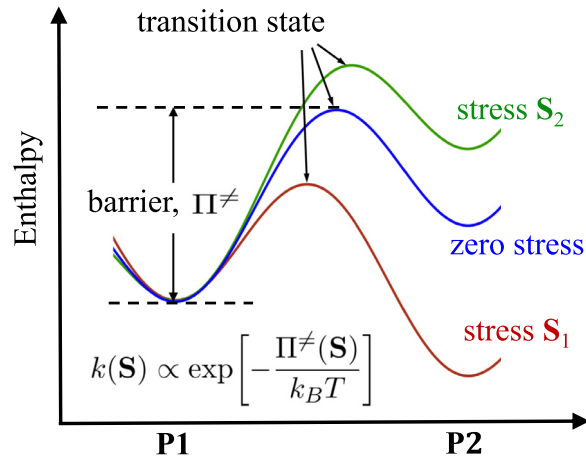*E-mail address:* wei.gao@utsa.edu (W. Gao).

Fig. 1. Schematic of stress dependent minimum energy path (MEP). In the equation, k is transition rate, k_B is Boltzmann constant and T is temperature.

on the other side of MEP, making the transition from P2 to P1 easier. The phase transition rate also depends on the activation energy ($k_B T$), so increasing temperatures can help to overcome transition barriers. The phase transition of solids can be influenced by either engineering the barriers or varying the thermal excitation. At the meso or continuum level, phase transitions at finite temperatures can be simulated with thermodynamic methods such as the phase field method, where the parameters in these methods are usually related to the transition barriers. Therefore, the evaluation of stress dependent barriers is critical for modeling phase transitions.

Transition MEPs and barriers can be calculated by atomistic simulations using transition state search methods such as *nudged elastic band* (NEB) method. The conventional NEB (Jónsson et al., 1998) only takes atomic positions as transition variables. Hence, it can not be directly applied to study solid–solid transitions when lattice deformation and external stress field also contribute to the MEP. Moreover, solid–solid transitions are usually accompanied with finite lattice deformation. Recently, we developed a *finite deformation NEB* (FD-NEB) method (Ghasemi et al., 2019) for finding transition pathways of solids under finite deformation. FD-NEB was formulated by introducing finite deformation variables to the previous solid state NEB method (Sheppard et al., 2012).

In order to determine the barriers under many possible external stresses, a large number of FD-NEB simulations must be performed. To avoid such high computational cost, the approximate theory to estimate stress dependent barriers is needed. Unfortunately, there is no existing theory readily to be applied, while similar problems have been studied on force dependent chemical reactions in the field of *mechanochemistry* (Dudko et al., 2006; Konda et al., 2011; Kucharski and Boulatov, 2011; Ribas-Arino et al., 2009a). A commonly used method is *Bell theory* (Bell, 1978), which allows one to estimate chemical reaction barriers as a function of applied force using the reaction results calculated at zero force. However, the Bell theory was formulated on discrete atomic systems in terms of forces and displacements of atoms, so one cannot directly apply Bell theory to study phase transition of solid materials coupled with stress and deformation. In addition to the Bell theory, Zhu et al. (2005) provided a method to compute the energy barrier of a transition process under constant strain, where they used a perturbation analysis on the MEP for a generically defined reaction coordinate. In this paper, we propose a *finite deformation Bell theory* (FD-BT) developed based on the concept of original Bell theory and continuum mechanics, for predicting transition barriers as a function of the applied stress.

The remainder of this paper is organized as follows. In Section 2, we briefly introduce the idea of the Bell theory, followed by the formulation for the method of FD-BT. After that, a 1D example, which has exact analytical solutions, is used to demonstrate the application of the FD-BT. In Section 3, we briefly introduce the principle of the FD-NEB computational method, which can provide numerical validations to the FD-BT predictions. In Section 4, the FD-BT is applied to study the phase transitions of 2D $MoTe_2$ and bulk Si, where the theoretical predictions are compared with FD-NEB simulations. Some extended discussions are provided in Section 5. Finally, the paper is summarized in Section 6.

2. Finite deformation bell theory for solid–solid phase transition

2.1. Bell theory and limitations

The original Bell theory (Bell, 1978) was developed to describe the receptor-ligand dissociation rate under external forces for cell adhesion. Since then, it has been generalized to study the force dependent chemical reactions such as increased rate of chemical bond dissociation under external forces (Dudko et al., 2006; Kucharski and Boulatov, 2011; Ribas-Arino et al., 2009a). The idea of Bell theory can be illustrated by an example of ring opening of a Benzocyclobutene molecule, as shown in Fig. 2. In the case of no external force, the molecule has to overcome an energy barrier of $\mathcal{V}^{\neq}$ in order to
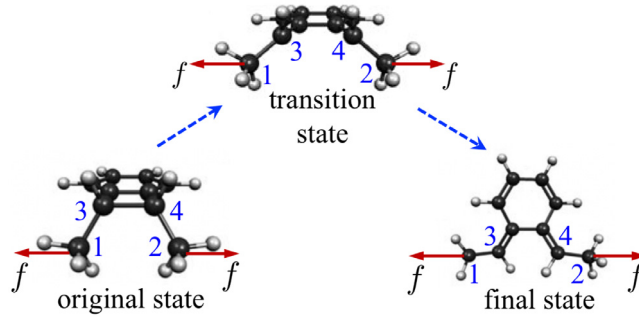
Fig. 2. Force dependent ring opening (3–4 bond) of Benzocyclobutene molecule. The figure is modified from Ribas-Arino et al. (2009b).

transform to the ring-opened (covalent bond between atoms 3 and 4) final state, where the transition rate $k \propto \exp(\mathcal{V}^{\neq}/k_B T)$. When a pair of external force f is applied on atoms 1 and 2, based on the Bell theory, the barrier is changed by $-f\Delta R_{12}$ where $\Delta R_{12} = R_{12}^{(t)} - R_{12}^{(o)}$ is the difference in distance between atoms 1 and 2 from original (o) to transition (t) state, thus the reaction rate becomes $k(f) \propto \exp[(\mathcal{V}^{\neq} - f\Delta R_{12})/k_B T]$. In the Bell theory, ΔR_{12} is approximated from the original and transition states at zero force. Hence, the Bell theory provides a linear approximation to force dependent chemical reaction barriers based on zero force atomistic calculations.

It can be noted that the Bell theory was formulated on discrete molecular systems in terms of forces and displacements of atoms. To apply this method for studying stress dependent phase transition of solids, one has to convert stress to atomic forces, and deformation to atomic displacements. This process is rather complicated and infeasible in practice. Instead, we could directly bring in continuum mechanics variables and build the connections between stress and transition barriers, so that the stress dependent barriers can be predicted based on the barrier calculated at zero stress, similar to the concept of the Bell theory. Following this idea, a new theoretical approach is developed in the framework of continuum mechanics.

2.2. Formulation of finite deformation bell theory

Consider a phase change crystal material subjected to a constant second Piola–Kirchhoff (P–K) stress, denoted by **S**. The static enthalpy (which does not include kinetic energy) of the system, denoted by Π, can be written as

$$\Pi(\mathbf{S}) = \mathcal{V}(\mathbf{S}) - V_0 \, \mathbf{S} : \mathbf{E}(\mathbf{S}), \tag{1}$$

where $\mathcal{V}$ is the potential energy of the system, V_0 is the initial lattice volume, **E** is the Green-Lagrangian strain with respect to the original zero stress state, and the inner product (represented by ": ", implying a double contraction on tensors) of **S** and **E** gives the work done by the stress. The enthalpy difference between the original and transition states gives the transition barrier

$$\Pi^{\neq}(\mathbf{S}) = \Pi^{(t)}(\mathbf{S}) - \Pi^{(o)}(\mathbf{S}), \tag{2}$$

where (o) and (t) respectively represent the original and transition state. The stress dependent phase transition rate can be calculated by the transition state theory. A harmonic approximation can be applied to simplify the transition state theory for crystal materials when the temperature of interest is low compared with the melting temperature of the materials (Olsen, 2006). Then, the stress dependent phase transition rate is written as

$$k(\mathbf{S}) = \nu \, \exp\left[-\frac{\Pi^{\neq}(\mathbf{S})}{k_B T} \right], \tag{3}$$

where the prefactor ν depends on the atomic vibrational frequency at the original and transition states (Hanggi et al., 1990; Olsen, 2006). The period of a typical atomic bond-stretch vibration is on the order of 0.1 ps, thus yielding a prefactor on the order of 10^{13} s^{-1}. Since $k(\mathbf{S})$ is exponentially dependent on the barrier, it is reasonable to neglect the much weaker stress dependence of the prefactor. Once $\Pi^{\neq}(\mathbf{S})$ is known, one can use Eq. (3) to calculate transition rate at temperature T. This rate can be taken as an important parameter for thermodynamic modeling of phase transitions at the larger length scales.

Fig. 3 describes the relationship between two phase transitions, occurring respectively under zero stress (I $\rightarrow$ III) and under stress **S** (II $\rightarrow$ IV), where I, II, III and IV represent four different states. The schematic lattice cells with two atoms in the figure are used to demonstrate the lattice deformation and atoms movements during transitions. The deformation measurements of different states are defined in the figure. A Green-Lagrangian strain tensor $\mathbf{E}^{(t)}(0)$ describes the deformation due to phase transition at zero stress. The deformations from state I to states II and IV are respectively described by $\mathbf{E}^{(o)}(\mathbf{S})$ and $\mathbf{E}^{(t)}(\mathbf{S})$. The latter one includes the contributions from both elastic deformation and phase transition. The purpose of the proposed theory is to predict the barrier $\Pi^{\neq}(\mathbf{S})$ under stress **S** using the zero stress barrier $\Pi^{\neq}(0)$.

Substitute Eq. (1) into Eq. (2), the barrier for phase transition at stress **S** can be written as

$$\Pi^{\neq}(\mathbf{S}) = \mathcal{V}^{(t)}(\mathbf{S}) - \mathcal{V}^{(o)}(\mathbf{S}) - V_0 \, \mathbf{S} : (\mathbf{E}^{(t)}(\mathbf{S}) - \mathbf{E}^{(o)}(\mathbf{S})). \tag{4}$$
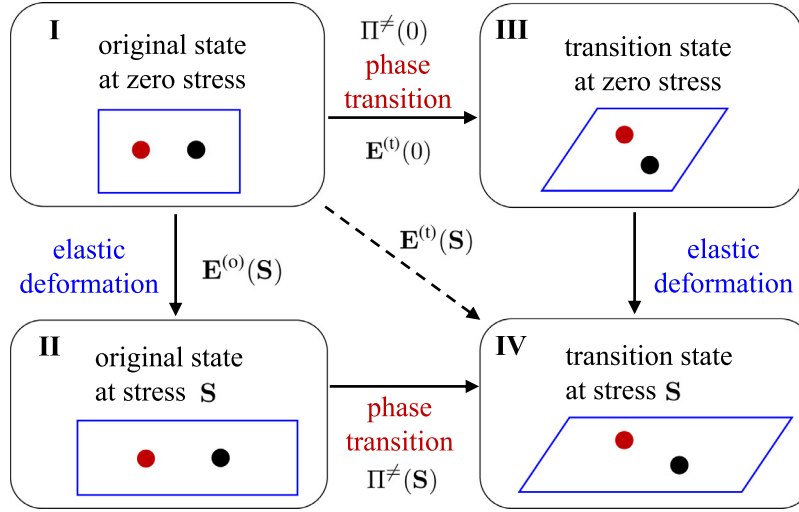
Fig. 3. Schematic relationship between the transitions under zero stress and under stress **S**. The blue box represents a crystal lattice with 2 atoms. (For interpretation of the references to color in this figure legend, the reader is referred to the web version of this article.)

At both original and transition states (II and IV in Fig. 3), we can expand the potential energies in a Taylor series around zero stress and neglect the terms higher than the second order

$$\mathcal{V}^{(o),(t)}(\mathbf{S}) = \mathcal{V}^{(o),(t)}(0) + \mathbf{S} : \frac{\partial \mathcal{V}^{(o),(t)}(0)}{\partial \mathbf{S}} + \frac{1}{2}\mathbf{S} : \frac{\partial^2 \mathcal{V}^{(o),(t)}(0)}{\partial \mathbf{S}^2} : \mathbf{S} + \mathcal{O}(\mathbf{S}^3). \tag{5}$$

This expansion is to build the connection between potential energies $\mathcal{V}$ at zero stress and at stress **S**, for both original state (I $\rightarrow$ II) and transition state (III $\rightarrow$ IV).

Since both original and transition states (II and IV) are in equilibrium, the variation of enthalpy equals zero, $\delta \Pi^{(o),(t)}(\mathbf{S}) = 0$, then from Eq. (1) we can get

$$\mathbf{S} = \frac{1}{V_0} \frac{\partial \mathcal{V}^{(o),(t)}}{\partial \mathbf{E}^{(o),(t)}}. \tag{6}$$

Using this relationship, the first and second order derivatives of $\mathcal{V}$ can be written as

$$\frac{\partial \mathcal{V}^{(o),(t)}}{\partial \mathbf{S}} = V_0 \, \mathbf{S} : \frac{\partial \mathbf{E}^{(o),(t)}}{\partial \mathbf{S}}, \tag{7}$$

and

$$\frac{\partial^2 \mathcal{V}^{(o),(t)}}{\partial \mathbf{S}^2} = V_0 \left[\mathbf{I} : \frac{\partial \mathbf{E}^{(o),(t)}}{\partial \mathbf{S}} + \mathbf{S} : \frac{\partial^2 \mathbf{E}^{(o),(t)}}{\partial \mathbf{S}^2} \right], \tag{8}$$

where **I** is the fourth order identity tensor. Substitute Eqs. (7) and (8) into Eq. (5) at $\mathbf{S} = 0$, we can get

$$\mathcal{V}^{(t)}(\mathbf{S}) - \mathcal{V}^{(o)}(\mathbf{S}) = \mathcal{V}^{(t)}(0) - \mathcal{V}^{(o)}(0) + \frac{V_0}{2}\mathbf{S} : \left[\frac{\partial \mathbf{E}^{(t)}(0)}{\partial \mathbf{S}} - \frac{\partial \mathbf{E}^{(o)}(0)}{\partial \mathbf{S}} \right] : \mathbf{S} + \mathcal{O}(\mathbf{S}^3). \tag{9}$$

Meanwhile, we can Taylor expend the strains $\mathbf{E}^{(o),(t)}(\mathbf{S})$ at zero stress to the first order and get

$$\mathbf{E}^{(t)}(\mathbf{S}) - \mathbf{E}^{(o)}(\mathbf{S}) = \mathbf{E}^{(t)}(0) - \mathbf{E}^{(o)}(0) + \mathbf{S} : \left[\frac{\partial \mathbf{E}^{(t)}(0)}{\partial \mathbf{S}} - \frac{\partial \mathbf{E}^{(o)}(0)}{\partial \mathbf{S}} \right] + \mathcal{O}(\mathbf{S}^2), \tag{10}$$

which is then substitute into Eq. (4) along with Eq. (9), yielding the barrier at stress **S**

$$\Pi^{\neq}(\mathbf{S}) = \Pi^{\neq}(0) - V_0\mathbf{S} : (\mathbf{E}^{(t)}(0) - \mathbf{E}^{(o)}(0)) - \frac{V_0}{2}\mathbf{S} : \left[\frac{\partial \mathbf{E}^{(t)}(0)}{\partial \mathbf{S}} - \frac{\partial \mathbf{E}^{(o)}(0)}{\partial \mathbf{S}} \right] : \mathbf{S} + \mathcal{O}(\mathbf{S}^3), \tag{11}$$

where $\Pi^{\neq}(0) = \mathcal{V}^{(t)}(0) - \mathcal{V}^{(o)}(0)$ is the barrier at zero stress, and $\mathbf{E}^{(o)}(0) = 0$ for zero stress reference state.

In Eq. (11), a linear dependence of the barrier on the applied stress can be considered as a generalization of the Bell theory in terms of a continuum description. In addition, a nonlinear response comes from the second order term, whose coefficients correspond to the difference of material's compliances between transition and original states. To estimate the barriers with Eq. (11), one firstly needs to use transition state search methods such as FD-NEB to get the barrier $\Pi^{\neq}(0)$ and

the strain $\mathbf{E}^{(t)}(0)$ of transition state at zero stress. For the second order correction, one needs to calculate the material compliances of both original and transition states. This can be done through molecular statics simulations. Since transition states are metastable, a second-order optimization method such as quasi-Newton algorithm may be needed, which only searches the energy minima in the vicinity of the transition states in order to avoid large perturbations during optimization process. It is noted that, the higher order corrections to the barrier beyond the second order may be needed, when materials exhibit strong nonlinearity at original or transition state. This could be done by taking the higher orders of $\mathcal{V}$ and $\mathbf{E}$ expansions, which will lead to the calculations of higher order material stiffness or compliance for both original and transition states.

Here, the theory is formulated using the second P–K stress which has mathematical advantages for describing materials constitutive behavior. Alternatively, following the same process, one can also derive Eq. (11) in terms of the first P–K stress along with the deformation gradient, which form a work conjugate pair. One advantage of using the first P–K stress is that it can be experimentally measured when the applied force is known, making the direct comparison between the theory and experiments easier. On the other side, it is not convenient to use Cauchy stress for describing the stress dependent barrier when the transition undergoes finite deformation, because Cauchy stress is not a work conjugate to any kind of strain, making it difficult to write down the work as shown in Eq. (1). However, there is a special case – the hydrostatic compression, where the Cauchy stress (the pressure p) is a constant, so the work is simply $p\Delta V$ where ΔV is the volume change.

There is one situation that needs particular attention when applying the proposed method. The expansion in Eq. (5) is to build the connection between potential energies $\mathcal{V}$ at zero stress and stress $\mathbf{S}$, for both original state (I $\rightarrow$ II) and transition state (III $\rightarrow$ IV). Such expansion is always meaningful for the original state. However, it is only meaningful for the transition state when the following condition is satisfied: the configuration of state III can be mapped to the configuration of state IV through an elastic deformation. Otherwise, the term $\mathcal{V}^{(t)}(0)$ on the right hand side of Eq. (5) cannot be used to represent the actual transition state at zero stress (III). The above condition is approximately true when the phase transition pathway under stress $\mathbf{S}$ is similar to the one under zero stress. However, such condition may not be satisfied when the transition mechanism changes beyond a certain stress. In these cases, the following additional steps have to be added in order to apply the proposed theory. First, the critical stress at which the transition mechanism starts to change has to be identified from atomistic simulations such as FD-NEB. Then, this critical stress state is taken as a new reference state (instead of zero stress state) to predict the barriers beyond such stress, following the similar process described above. In this way, the theory will be applied in a piecewise manner, where the different stress regions are separated by the critical stresses at which the transition mechanism starts to change.

Microscopically, the above elastic mapping assumption for transition state can be interpreted as follows: the displacements of atoms from configuration III to IV follow Cauchy-Born rule (Born and Huang, 1954; Tadmor and Miller, 2011), which states that the displacements of atoms are set by a deformation gradient plus an internal relaxation associated with the relative motion of sublattices. In reality, in addition to the displacements set by Cauchy-Born rule, there may be extra atomic displacements coming from phase transition. These extra displacements could be considered in our formulation implicitly by adding the reaction coordinate (which include both lattice deformation and atomic displacements) as a control variable, similar to the approach used by Zhu et al. (2005). However, the reaction coordinate is not an explicit variable that can be conveniently computed in theory. Therefore, our current formulation is kept simple for the purpose of easy implementation.

2.3. A simple example: "Phase Transition" of a 1D chain

Consider a fictitious 1D chain composed by a series of beads as shown in Fig. 4a. At the original state, the equilibrium distance between two neighboring beads is x_0. This distance is changed by x when a force f is applied. It is assumed that all the beads are always equally spaced when they are subjected to stretch or compression. The interaction energy between two neighboring beads is described by a Cosine function

$$\mathcal{V}(x) = -\cos(2\pi x), \tag{12}$$

where $-0.5 \leq x \leq 1.5$. Then, under the force f, the enthalpy of the system can be written as

$$\Pi(x) = \mathcal{V}(x) - fx. \tag{13}$$

Note that all the physical quantities used in this example are unitless for the convenience of discussion.

The enthalpy profiles of the system at $f = 0$ and $f = \pm 0.6$ are shown in Fig. 4b. There are two possible stable states: one is at the left valley around original state ($x = 0$), the other one is around the right valley ($x = 1$) across an "energy barrier". Interestingly, the barrier shifts up and down depending on the direction and magnitude of the applied force f. From $d\Pi/dx = 0$, the positions of the original (o) and transition (t) states can be evaluated as a function of f

$$x^{(o)}(f) = \frac{1}{2\pi} \arcsin\left(\frac{f}{2\pi}\right) \quad \text{and} \quad x^{(t)}(f) = \frac{1}{2} - \frac{1}{2\pi} \arcsin\left(\frac{f}{2\pi}\right). \tag{14}$$

Substitute Eq. (14) into Eq. (13), we can obtain the exact values of barrier $\Pi^{\neq}$ as a function of f, which are plotted as the solid line in Fig. 4c. Meanwhile, the barrier can be estimated using the proposed theory. Based on Eq. (11), the barrier can
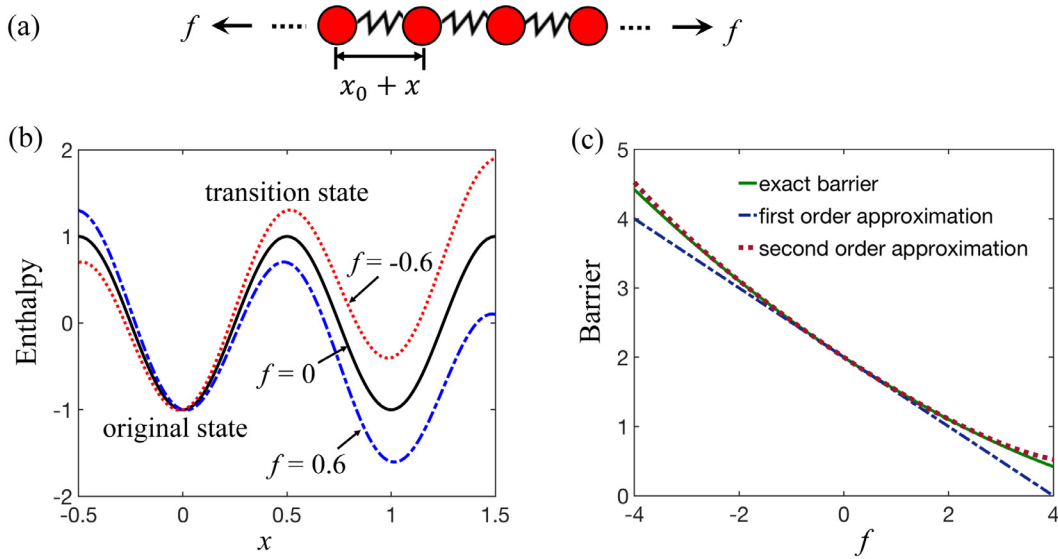
Fig. 4. (a) A chain made by series of beads. The equilibrium distance between two beads is x_0, and the deformation under force f is x. (b) Enthalpy profiles between two neighboring beads at different forces. (c) Comparisons of transition barrier between exact values and approximated ones.

be written as

$$\Pi^{\neq}(f) = \Pi^{\neq}(0) - f[x^{(t)}(0) - x^{(0)}(0)] - \frac{1}{2}f^2\left[\frac{dx^{(t)}(0)}{df} - \frac{dx^{(o)}(0)}{df}\right], \tag{15}$$

where $x^{(0)}(0) = 0$ and $x^{(t)}(0) = 1/2$, and from $d\Pi^{(o),(t)}/dx = 0$, the second order coefficients can be written as

$$\frac{dx^{(o),(t)}(0)}{df} = \frac{1}{\mathcal{V}^{(o),(t)''}(0)}, \tag{16}$$

which describes the compliance of the 1D system. In this example, because $\mathcal{V}^{(o)}(0)'' > 0$ and $\mathcal{V}^{(t)}(0)'' < 0$, the second order contribution is always positive, so increasing the value of barriers with respect to the first order approximation. However, this cannot be generalized to multidimensional material systems in which the second order term can be either positive or negative, as shown in the examples in Section 4.

The barriers of this fictitious 1D system are exactly evaluated, while for a real phase change material, the barrier needs to be calculated from atomistic simulations using transition state search methods such as finite deformation NEB (FD-NEB) method. In next section, we briefly introduce the principle of FD-NEB method, which was developed recently for determining transition paths and barriers of solid-state materials under finite deformation.

3. Atomistic simulation method: finite deformation nudged elastic band method

Molecular dynamics (MD) simulations are widely used to study the mechanical behavior of solids by accounting for the motion of atoms. However, the phase transitions of interest can be many orders of magnitude slower than vibrations of the atoms, so a direct MD simulation may not be feasible due to the limitation on the accessible simulation time scale. For example, the transition rate of a phase transition process with a barrier of 0.6 eV can be calculated as $k = 834$ s^{-1} with Eq. (3) where ν is taken as 10^{13} s^{-1} at $T = 300$ K. Thus, the average time one needs to wait to observe this transition event is $\Delta t = 1/k = 1.2$ ms. This time scale is far beyond the capability of present day computers, so such transition event is not observable in MD simulations. Therefore, many methods have been developed to accelerate MD simulations (Miron and Fichthorn, 2003; Voter, 1997; Xu and Henkelman, 2008), however it is still challenging to access such long time scales, especially for large size systems or when the energy and force are evaluated with first principle methods. On the other hand, the indirect simulation method – transition state search methods, such as nudged elastic band (NEB), have been used to study transition events. Given the initial and final states of a transition process, the NEB method can be used to find the minimum energy path (MEP).

The conventional NEB (Jónsson et al., 1998; Mills et al., 1995) only takes atomic positions as transition variables, so it can not be directly applied to study solid–solid transitions where lattice deformation and external stress field also contribute to the search of MEP. Solid-state NEB methods have been proposed to include the influence of lattice deformation and stress. Recently, we noticed that the previous solid-state NEB algorithm leads to inaccurate barriers and deviated transition paths, due to an inaccurate evaluation on the external work contributions in enthalpies and barriers. To this end, a finite
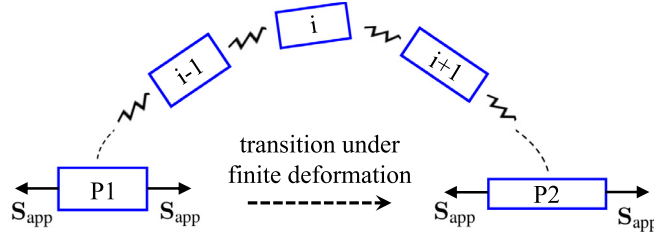
Fig. 5. Schematics of FD-NEB calculation from phase P1 to P2. Blue boxes represent lattice cells.

deformation NEB (FD-NEB) method (Ghasemi et al., 2019) was formulated by adding finite deformation variables to previous solid-state NEB method (Sheppard et al., 2012). In addition to the FD-NEB, a pioneering work by Huang et al. (2009) provided a stress-controlled NEB method which was applied to study the nanoscale fracture mechanisms in silicon.

The FD-NEB calculation can be illustrated in Fig. 5, where a crystal material (the lattice is represented by a blue box) transforms from phase P1 to P2 when it is subjected to a constant stress S_{app}. To describe the finite deformation of the lattice during phase transition, nonlinear mechanics variables are used to control the search of MEP. FD-NEB can be formulated with either first or second P–K stress in a similar way. To be consistent with our formulation of FD-BT theory, here we present the idea of FD-NEB with the second P–K stress. As shown in Fig. 5, a band is initially constructed by connecting a number of intermediate states between the given initial and final states with elastic springs. These intermediate states are usually generated by a geometric linear interpolation between the initial and final states as an initial guess. The purpose of FD-NEB algorithm is to move the elastic band until it converges to the MEP under stress S_{app}.

For a material containing N atoms, each state on the elastic band has $3N$ atomic degrees of freedom. None of the intermediate states are in equilibrium due to phase transition, so they are subjected to the *potential forces* coming from the gradient of the potential energy $\boldsymbol{f}^i_{pot} = -\nabla \mathcal{V}(\boldsymbol{r}^i_1, \boldsymbol{r}^i_2, \cdots, \boldsymbol{r}^i_N)$, where $\boldsymbol{r}$ represents atomic positions. The superscript i represents ith state along the elastic band. Minimizing these forces only moves the intermediate states into one of the local energy minima, and thus would not help to find the MEP. Therefore, spring forces are applied in order to keep the intermediate states evenly spaced on the elastic band. To avoid the sensitivity of selecting spring constant values for convergence, only certain components of the forces are used. Specifically, the total force of an intermediate state i is

$$\boldsymbol{f}^i = \boldsymbol{f}^i_{pot}|_\perp + \boldsymbol{f}^i_{spr}|_\parallel, \tag{17}$$

where $\boldsymbol{f}^i_{pot}|_\perp$ is the potential force perpendicular to the elastic band and $\boldsymbol{f}^i_{spr}|_\parallel$ is the spring force parallel to the band.

In addition to atomic degrees of freedom, the finite lattice deformation is also added to MEP search. When subjected to the external stress, an internal restoring stress is generated inside the lattice. This stress does not equal the applied stress, since the intermediate states are not in equilibrium. Hence, similar to atomic degrees of freedom, spring stress is prescribed between neighboring states. It is noted that the internal restoring stress, calculated from atomic simulations (by either empirical potentials or first-principles methods), is the Cauchy stress defined in current configuration. Therefore, in FD-NEB, the prescribed P-K stress (S_{app}) is converted to a Cauchy stress (σ^i_{app}). Then, the total stress acting on the lattice of intermediate state i is

$$\sigma^i = (\sigma^i_{app} - \sigma^i_{cell})|_\perp + \sigma^i_{spr}|_\parallel. \tag{18}$$

where σ^i_{cell} and σ^i_{spr} denote the restoring and spring stress respectively. In order to treat the atomic and cell variables on an equal footing, $\sigma_{app} - \sigma^i_{cell}$ and σ^i_{spr} are respectively vectorized and combined with $\boldsymbol{f}^i_{pot}$ and $\boldsymbol{f}^i_{spr}$ to form a generalized force vector. The atomic positions and cell geometries are simultaneously updated by this generalized force vector using any force-based optimization algorithms (Sheppard et al., 2008) until the MEP is converged. Finally, the transition barrier ($\Pi^{\neq}$) is calculated by the enthalpy difference between the original and transition states

$$\Pi^{\neq}(\boldsymbol{S}_{app}) = \mathcal{V}^{\neq}(\boldsymbol{S}_{app}) - V_0 \boldsymbol{S}_{app} : (\boldsymbol{E}^{(t)} - \boldsymbol{E}^{(o)}), \tag{19}$$

where $\mathcal{V}^{\neq}$ is the potential energy difference between transition and initial states, $\boldsymbol{E}^{(t)}$ and $\boldsymbol{E}^{(o)}$ are respectively the Green-Lagrangian strain tensors of transition and original states under stress $\boldsymbol{S}_{app}$ with respect to the reference state (whose volume is V_0). For convenience, the original state under zero stress is selected as the reference state in FD-NEB.

A large number of FD-NEB simulations are needed in order to obtain the barriers at different stress fields. These calculations are computationally costly if the forces and stresses are calculated from first-principle methods. Therefore, it is meaningful to use the proposed FD-BT theory as a guide to explore the entire stress space and then use FD-NEB for validation at selected stress levels.

4. Examples

In this section, the FD-BT is applied to calculate the stress dependent barriers of phase transitions of 2D $MoTe_2$ and bulk silicon, which exhibit two distinct transition mechanisms. Meanwhile, the theoretical predictions are compared with
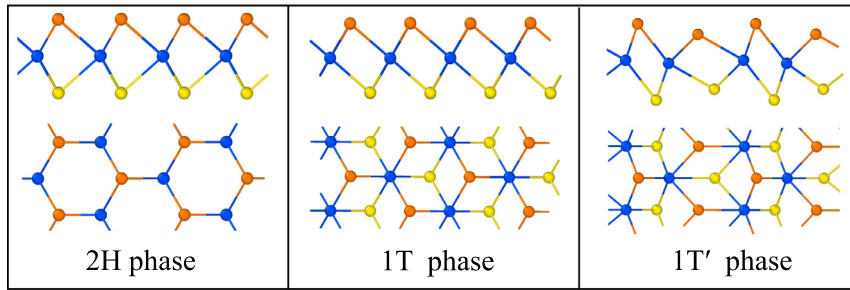
Fig. 6. Cross-sectional and basal plane views of 2D MoTe$_2$ at different phases. Blue color: Mo; orange/yellow color: Te atoms on the top and bottom layers. (For interpretation of the references to color in this figure legend, the reader is referred to the web version of this article.)

atomistic simulations with FD-NEB. In the simulations, the energy, interatomic force and stress are evaluated from the density functional theory (DFT). All the DFT calculations in this study are performed using the plane-wave-based Vienna Ab-initio Simulation Package (VASP) (Kresse and Furthmüller, 1996; Kresse and Hafner, 1993). Electron exchange and correlation energies are calculated with the generalized gradient approximation using the Perdew–Burke–Ernzerhof (PBE) functional (Perdew et al., 1996). The projector augmented wave (PAW) method (Blöchl, 1994; Kresse and Joubert, 1999) is used to represent ionic cores. The kinetic energy cutoff for the plane-wave basis describing the valence electrons is set to 292 eV and 420 eV respectively for MoTe$_2$ and silicon, and the corresponding k-point used to sample Brillouin zones are 7 × 9 × 1 and 15 × 15 × 15. A vacuum layer of thickness 3 nm is used to separate the periodic images of MoTe$_2$ sheet.

4.1. Phase transition of 2D MoTe$_2$

As shown in Fig. 6, the monolayer MoTe$_2$ in 2H phase is composed of a layer of hexagonally arranged Mo atoms, sandwiched between two layers of Te atoms. 2H phase is semiconductor with a direct band gap. When one of the Te layers in 2H phase is shifted, the Te atoms are in octahedral coordination around Mo atoms, generating a 1T phase. 1T structure is unstable in the absence of external stabilizing factors. As a result, it turns into monoclinic and conducting 1T′ phase, a distorted version of the 1T structure. MoTe$_2$ has a lower ground state energy at 2H phase (Duerloo et al., 2014). The dynamic control of transitions between these two phases can lead to revolutionary device applications such as memory devices (Wuttig and Yamada, 2007), reconfigurable circuits (Wang et al., 2016) and topological transistors (Qian et al., 2014) at atomically thin limits.

A recent experiment showed that nanoindentation applied by Atomic Force Microscope can induce phase transition on suspended MoTe$_2$ thin films at ambient condition (Song et al., 2016). In addition, the phase transition of monolayer MoS$_2$ and MoTe$_2$ has been experimentally reported through chemical/thermal doping (Lin et al., 2014; Ma et al., 2015), laser patterning (Cho et al., 2015) and electrostatic gating (Wang et al., 2017), where stress plays an important role due to thermal expansion, lattice mismatches and interactions with substrates. So far, the theoretical and computational studies on phase transition of 2D TMDC are quite limited. Particularly, the role of stress field on the transition barriers has not been explored.

The uniaxial tensile loading along armchair direction is considered in present study. Fig. 7 shows the stress-strain curves of monolayer MoTe$_2$ obtained from molecular statics simulations, in which the sheet is stretched on armchair direction while relaxing stress on the other two directions. For 2D materials, we use 2D stress (unit: N/m) tensor, which have 3 independent components: S_{11}, S_{22} and S_{12}. The 2H and 1T′ phases at zero stress are respectively represented by a_0 and b_0. Note that the strains are all measured with respect to state a_0, so the strain of 1T′ phase at zero stress is not zero. The purpose of the FD-BT is to predict the barrier of the transition $a \rightarrow b$ under stress based on the information of the transition $a_0 \rightarrow b_0$. It is worth pointing out that, there was no sign of phase transition before failure during the stretching of the 2H phase (through stress or strain control), meaning that the transition is not expected to occur only by stretching when there is no thermal activation.

The application of FD-BT requires the inputs from zero-stress phase transition, as shown in Eq. (11), including the barrier $\Pi^{\neq}(0)$, the strain of transition state $\mathbf{E}^{(t)}(0)$, as well as the tangent compliances $\mathbf{c}^{(o),(t)}(0) = \partial \mathbf{E}^{(o),(t)}(0)/\partial \mathbf{S}$ of both original and transition states which are needed for the second order correction. Therefore, zero-stress FD-NEB simulation was firstly performed. The obtained MEP curve is shown in Fig. 8a, where the reaction coordinate of MEP represents the distance between two neighboring states on the elastic band in terms of both atom positions and lattice deformation. The snapshots in Fig. 8b describe atomic motions during the transition process. In the beginning of the transition process, one Te atom in the bottom layer (yellow color) shifts out toward the center of 2H hexagon; meanwhile other atoms are slightly displaced from their original positions, leading to the transition state represented by B. The difference of enthalpies between this transition state and the original state gives the transition barrier (which has to be overcome to initiate the transition). Beyond this point, a shallow minimum appears on the MEP at C, indicating a stable intermediate phase. Finally, another Te atom in the bottom layer moves out by overcoming a small barrier at D, completing the transition process.
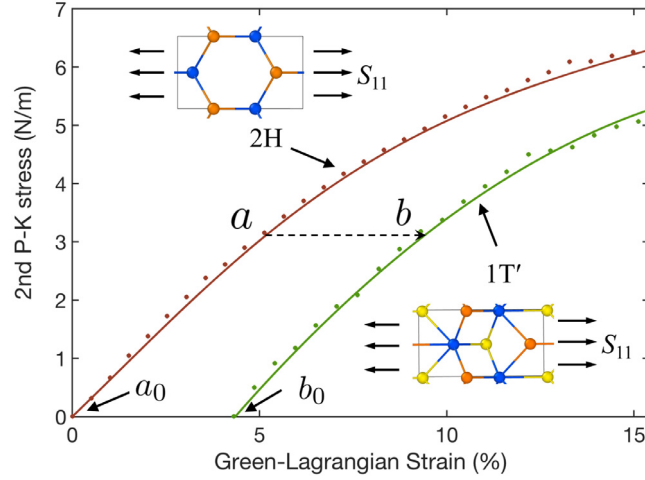
Fig. 7. Stress–strain relationships of monolayer MoTe$_2$ at 2H and 1T′ phases, stretched on armchair direction, where the strain is measured with respect to zero stress 2H phase. The solid curves are calculated from the derivatives of potential energy. The inserted images show the unit cells used in simulations.
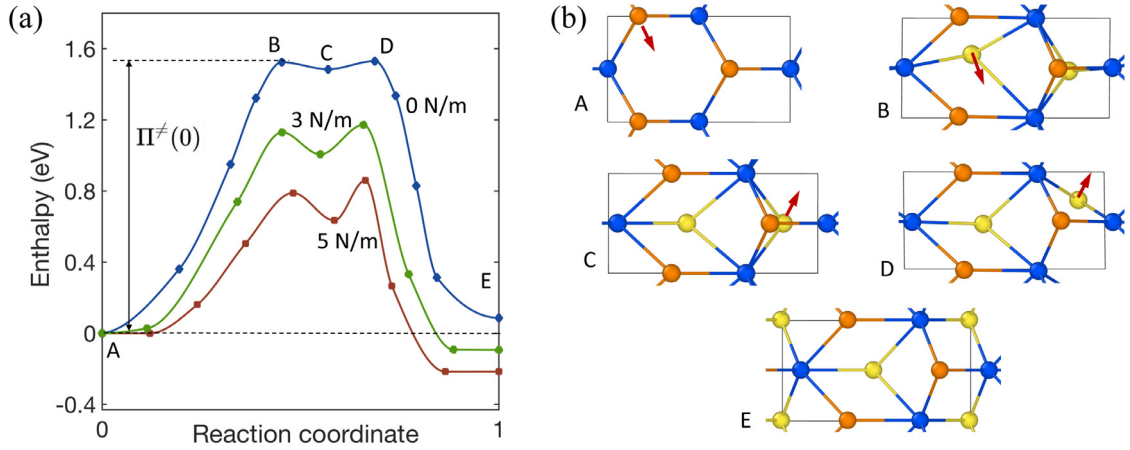

Fig. 8. (a) Phase transition MEPs of MoTe$_2$ obtained from FD-NEB calculations, where the enthalpy is calculated for the computation cell. (b) The snapshots show the atomic motion during transition process, where the box represents the computation cell. The lattice constants for stress free 2H and 1T′ structures are respectively 6.15 Å × 3.56 Å and 6.40 Å × 3.42 Å.

FD-NEB simulations were also performed to get barriers at different stress levels. The MEP curves under 3 N/m and 5 N/m are shown in Fig. 8a. The barrier drops with the increase of applied stress, meaning that a stretch on armchair direction facilitates the phase transition of monolayer MoTe$_2$. The atomic motions during the transitions under stress are similar to those of zero stress; meanwhile the intermediate phase at C becomes more stable as the increase of tensile stress.

Next, the information obtained from zero stress simulation are taken as inputs to FD-BT for predicting the barriers as a function of applied stress. For an uniaxial stress applied on armchair direction, Eq. (11) can be simplified as a function of the applied stress S_{11}

$$\Pi^{\neq}(S_{11}) = \Pi^{\neq}(0) - A_0 E_{11}^{(t)}(0)S_{11} - \frac{A_0}{2}(c_{11}^{(t)}(0) - c_{11}^{(o)}(0))S_{11}^2 + \mathcal{O}(S_{11}^3), \qquad (20)$$

where A_0 is the area of monolayer 2H MoTe$_2$ sheet at zero stress. The barrier $\Pi^{\neq}(0)$ (shown in Fig. 8a) and the strain $E_{11}^{(t)}(0)$ are the direct outputs from FD-NEB simulation under zero stress. The tangent compliance of 2H phase $c_{11}^{(o)}(0)$ is calculated from the stress-strain curve plotted in Fig. 7. In addition, the tangent compliance of transition state $c_{11}^{(t)}(0)$ can be obtained from molecular statics simulations. An uniaxial tensile simulation was performed on the structure of transition state (represented by B in Fig. 8b). The stress-strain curve of the transition state under uniaxial stress is shown in Fig. 9a. Note that the transition state is metastable, so a quasi-Newton algorithm is used for optimization, which only searches the structures of energy minima in the vicinity of this transition state. Here, only the initial portion of the curve is used to get the second order tangent stiffness at zero stress, while the whole curve may be useful to get the higher order stiffness if one extends the formulation of FD-BT by including higher order corrections beyond the second order. The parameters
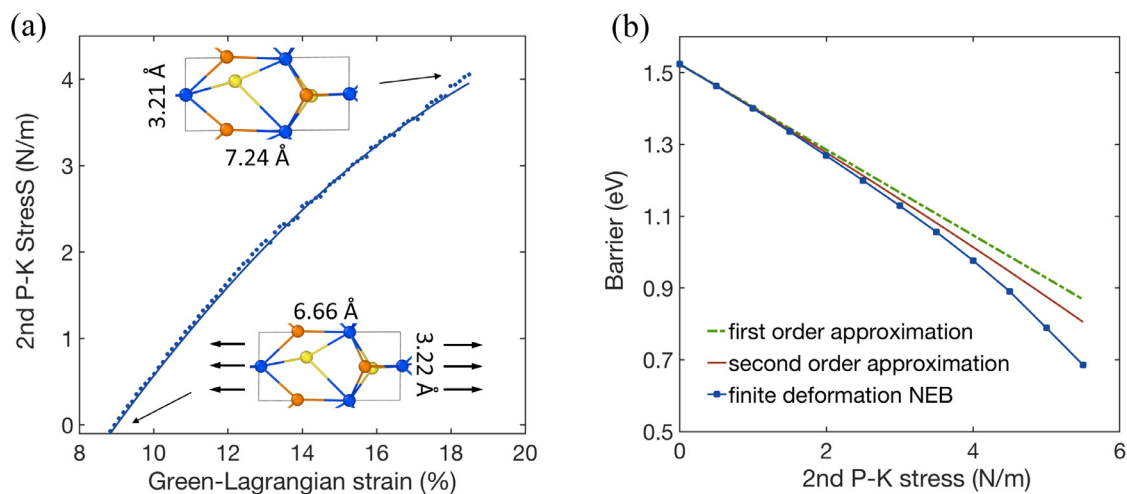
Fig. 9. (a) Stress–strain curves for transition state of MoTe$_2$ stretched on armchair direction, where the strain is measured with respect to zero stress 2H phase. The solid curve is calculated from the derivative of potential energy. (b) Comparison of the barriers of the computation cell as a function of applied stress.

Table 1
The parameters of original 2H and transition state (TS) used in Eq. (20) for predicting barriers under uniaxial stress. The units for energy, area and material compliance are respectively eV, Å^2 and cm/N.

Zero stress barrier $\Pi^{\neq}(0)$	2H area A_0	TS strain $E_{11}^{(t)}(0)$	TS compliance $c_{11}^{(t)}(0)$	2H compliance $c_{11}^{(o)}(0)$
1.52	21.86	8.74%	1.42	1.11

used in Eq. (20) are listed in Table 1. The theoretical predictions and simulation results are compared in Fig. 9b. While the theory overestimates the barrier, the estimation considerably improves by including the second order correction, where the compliance of the transition state is larger than that of the original state, so decreasing the barriers with respect to the first order approximation. The quality of prediction is related to the materials nonlinearity at original and transition states, and can be potentially improved by adding higher order corrections to Eq. (11).

4.2. Phase transition of silicon

At ambient conditions, the most stable phase of Si is a diamond structure. Under compressive stress, Si transforms from the diamond structure (Si-I) to a metallic β- tin structure (Si-II) and continually exhibits many other different phases with further increase of compression. Releasing loads does not lead to a recovery of the initial Si-I phase but instead to a series of metastable phases (Wippermann et al., 2016). These make phase transition of Si a rather complicated process, which still requires thorough investigations despite of the rich studies in the past decades. In this paper, we focus on the transition from Si-I to Si-II on a pristine Si structure.

First, we consider the phase transition under an uniaxial compression. Molecular statics simulations are conducted by using damped dynamics as a force-based optimizer, where the uniaxial compression is applied through a stress control. The stress-strain curves are shown in Fig. 10. At the peak stress (16.0 GPa), Si-I directly transforms to Si-II through a strain burst due to lattice instability. Different from the transition of MoTe$_2$ that is accompanied with the breaking of covalent bonds, the transition of Si only involves lattice deformation and atoms rearrangement. The peak stress of Si-I (16.0 GPa) in Fig. 10 can be considered as the upper bound of transition stress, because it triggers phase transition without the need of thermal activation. In reality, thermal energy can lower the transition stress, facilitating the material's ability to overcome energy barrier.

Similar to the previous example, FD-NEB simulations are applied at selected stress levels to get transition barriers, which are then compared with the predictions from FD-BT. The representative MEPs at three different stresses are shown in Fig. 11a. The variation of the barriers as a function of the applied stress is shown in Fig. 11b. The FD-BT predictions with second order correction compare closely to simulation results. It is noted that, the compliance of the transition state at zero stress is a negative value, making the second order contribution in Eq. (11) positive and thereby increasing the value of barriers with respect to the first order approximation. The parameters used in Eq. (11) for barrier predictions are listed in Table 2, where $\Pi^{\neq}(0)$, V_0, $E_{33}^{(t)}(0)$ and $c_{33}^{(t)}(0)$ are used for uniaxial compression.
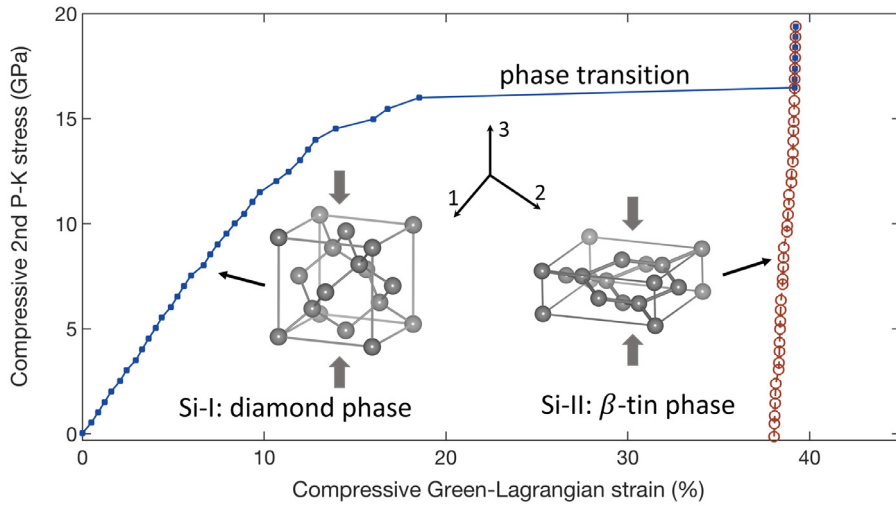
Fig. 10. Stress–strain curves (obtained from molecular statics simulations with stress control) of Si-I and Si-II under uniaxial compression, where the strain is measured with respect to zero stress Si-I. Phase transition occurs at the peak stress of Si-I due to lattice instability. The lattice structures shown in the figure are used for DFT calculations, where the lattice constants for stress free Si-I and Si-II structures are respectively 5.47 Å × 5.47 Å × 5.47 Å and 6.92 Å × 6.92 Å × 2.55 Å.
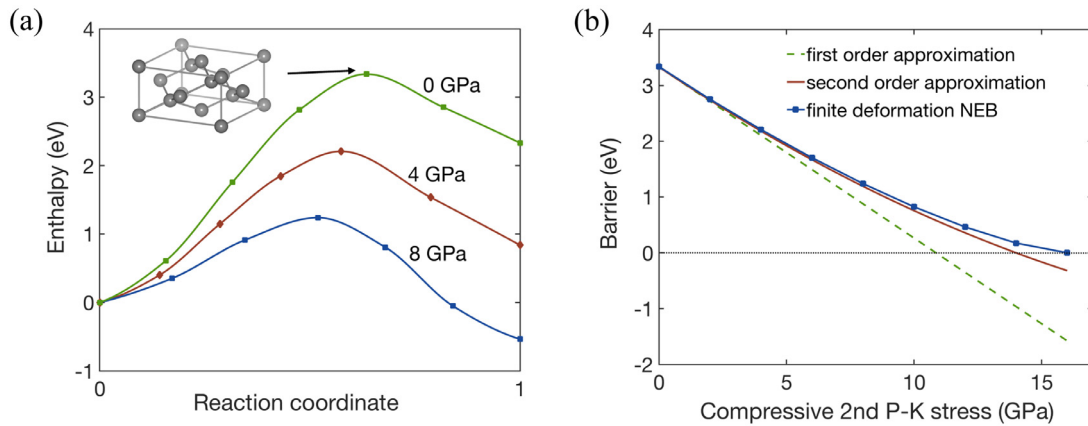

Fig. 11. (a) Si phase transition MEPs of at different stresses. The inserted crystal structure is for transition state at zero stress. (b) Barrier (of the computation cell) comparison between theoretical predictions and atomistic simulations.

Table 2
The parameters of original and transition state of Si used in Eq. (11) for predicting barriers under uniaxial compression and combined loading. The units for energy, volume and material compliance are respectively eV, Å^3 and TPa^{-1}.

$\Pi \neq (0)$	V_0	$E_{33}^{(t)}(0)$	$E_{11(22)}^{(t)}(0)$	$c_{33}^{(t)}(0)$	$c_{11(22)}^{(t)}(0)$	$c_{11(22,33)}^{(o)}(0)$
3.35	163.40	−29.66%	17.15%	-2.10	7.68	8.01

Next, we intend to use the theory to predict the barriers under combined loadings, where uniaxial compression is applied on one direction and equibiaxial tensions are applied on the other two directions. Using the parameters in Table 2, the barriers are calculated as a function of two stress components and plotted as contour lines in Fig. 12. On each contour line, we randomly select a point and compute the corresponding barrier with FD-NEB simulation. Similar to the case of uniaxial loading, the predictions are reasonably accurate at the small stresses but the difference gradually increases when the stress increases.

5. Discussion

It is noted that the transition process shown in both Si and MoTe$_2$ examples is *concerted transition*, where all the atoms transform to the new phase simultaneously. This is due to the confinement from the small periodic cells used in FD-NEB
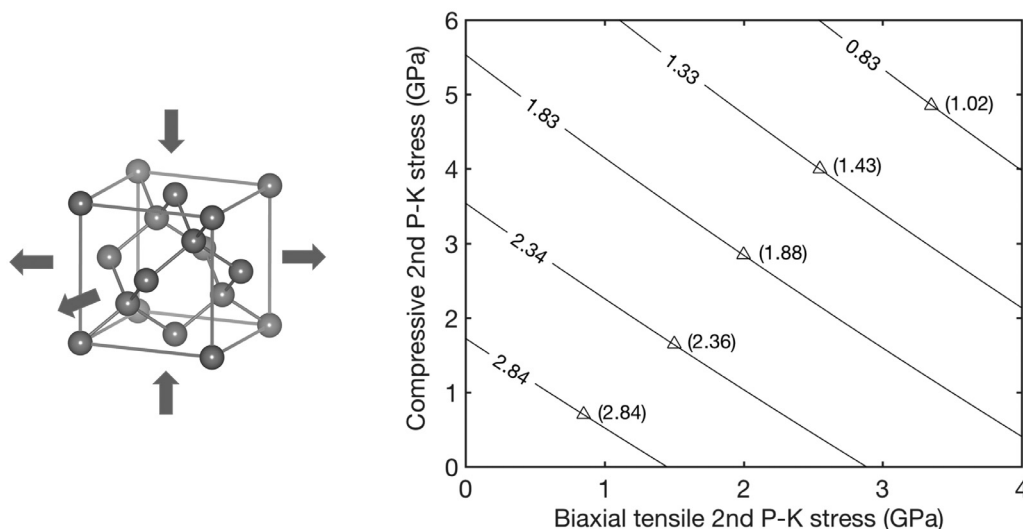
Fig. 12. The barrier (of the computation cell) contours of the transition from Si-I to Si-II under combined uniaxial compression and equibiaxial tension, predicted from FD-BT. Random points on the contour lines (marked by triangles) are selected for comparison with FD-NEB, and the values from simulations are shown inside parentheses.

simulations. By contrast, the other type of transition is *nucleated transition*, which starts from a localized site, followed by the propagation of the new phase. Both concerted and nucleated mechanisms could occur in reality depending on the materials and external excitations. It is indeed challenging to study nucleation-based phase transition with NEB method or other types of atomistic methods, because the nucleation volume may be greater than the size of computation cell. Moreover, the defects inside materials also play import roles in nucleation process. To avoid this complexity and computational constrains, we have chosen concerted nucleation examples to demonstrate the proposed theory.

As shown in the examples, the accuracy of the predicted barriers is material dependent. The Taylor expansion, conducted between undeformed and deformed states, is related to the elastic nonlinearity of the material. Silicon shows better predictions because of the weaker nonlinearity as compared to MoTe$_2$. It requires more studies in the future to quantitatively correlate the nonlinearity or some other potential factors to the accuracy of predictions.

6. Summary

Stress plays important role in solid–solid phase transitions and can be utilized as a useful tool in phase engineering applications. The mechanism of stress modulated phase transition is that the applied stress field can change the transition barrier which determines the likelihood of phase transition. The stress dependent barriers can be computed by using transition state search methods such as finite deformation nudged elastic band (FD-NEB) method. However, these methods are computationally expensive, so it is time consuming to find barriers under many different stresses. This paper presents a facile approach to quickly estimate the barriers in the entire stress space to certain accuracy. A finite deformation Bell theory (FD-BT) is developed to predict the stress dependent barriers using the information of zero-stress phase transition. The method is applied to study two model materials: 2D MoTe$_2$ and bulk silicon, and it is validated by comparing theoretical predictions to FD-NEB simulations. The two model materials demonstrate distinct transition mechanisms: 2D MoTe$_2$ experiences covalent bond breaking during transition while the transition of silicon is dominated by lattice instability. The barriers of both materials exhibit significant stress dependence, which can be reasonably predicted by FD-BT.

Declaration of Competing Interest

The authors declare that they have no known competing financial interests or personal relationships that could have appeared to influence the work reported in this paper.

CRediT authorship contribution statement

Arman Ghasemi: Methodology, Software, Investigation, Writing - original draft, Writing - review & editing. **Wei Gao:** Conceptualization, Methodology, Investigation, Writing - original draft, Writing - review & editing, Supervision, Funding acquisition.

Acknowledgments

References

Bell, G.I., 1978. Models for the specific adhesion of cells to cells. Science 200 (4342), 618–627.
Blöchl, P.E., 1994. Projector augmented-wave method. Phys. Rev. B 50 (24), 17953.
Born, M., Huang, K., 1954. Dynamical Theory of Crystal Lattices. Clarendon press.
Cho, S., Kim, S., Kim, J.H., Zhao, J., Seok, J., Keum, D.H., Baik, J., Choe, D.-H., Chang, K.J., Suenaga, K., Kim, S.W., Lee, Y.H., Yang, H., 2015. Phase patterning for ohmic homojunction contact in $MoTe_2$. Science 349 (6248), 625–628.
Dudko, O.K., Hummer, G., Szabo, A., 2006. Intrinsic rates and activation free energies from single-molecule pulling experiments. Phys. Rev. Lett. 96 (10), 108101.
Duerloo, K.-A.N., Li, Y., Reed, E.J., 2014. Structural phase transitions in two-dimensional Mo-and W-dichalcogenide monolayers. Nat. Commun. 5, 4214.
Ghasemi, A., Xiao, P., Gao, W., 2019. Nudged elastic band method for solid–solid transition under finite deformation. J. Chem. Phys. 151 (5), 54110.
Hanggi, P., Talkner, P., Borkovec, M., 1990. Reaction-rate theory - 50 years after Kramers. Rev. Modern Phys. 62 (2), 251–341.
Huang, S., Zhang, S., Belytschko, T., Terdalkar, S.S., Zhu, T., 2009. Mechanics of nanocrack: fracture, dislocation emission, and amorphization. J. Mech. Phys. Solids 57 (5), 840–850.
Jónsson, H., Mills, G., Jacobsen, K.W., 1998. Nudged elastic band method for finding minimum energy paths of transitions. In: Classical and Quantum Dynamics in Condensed Phase Simulations. World Scientific, pp. 385–404.
Konda, S.S.M., Brantley, J.N., Bielawski, C.W., Makarov, D.E., 2011. Chemical reactions modulated by mechanical stress: extended bell theory. J. Chem. Phys. 135 (16), 164103.
Kresse, G., Furthmüller, J., 1996. Efficient iterative schemes for ab initio total-energy calculations using a plane-wave basis set. Phys. Rev. B 54 (16), 11169.
Kresse, G., Hafner, J., 1993. Ab initio molecular dynamics for liquid metals. Phys. Rev. B 47 (1), 558.
Kresse, G., Joubert, D., 1999. From ultrasoft pseudopotentials to the projector augmented-wave method. Phys. Rev. B 59 (3), 1758.
Kucharski, T.J., Boulatov, R., 2011. The physical chemistry of mechanoresponsive polymers. J. Mater. Chem. 21 (23), 8237–8255.
Lin, Y.C., Dumcenco, D.O., Huang, Y.S., Suenaga, K., 2014. Atomic mechanism of the semiconducting-to-metallic phase transition in single-layered MoS_2. Nat. Nanotechnol. 9 (5), 391–396.
Ma, Y., Liu, B., Zhang, A., Chen, L., Fathi, M., Shen, C., Abbas, A.N., Ge, M., Mecklenburg, M., Zhou, C., 2015. Reversible semiconducting-to-metallic phase transition in chemical vapor deposition grown monolayer WSe2 and applications for devices. ACS Nano 9 (7), 7383–7391.
Mills, G., Jónsson, H., Schenter, G.K., 1995. Reversible work transition state theory: application to dissociative adsorption of hydrogen. Surf. Sci. 324 (2–3), 305–337.
Miron, R.A., Fichthorn, K.A., 2003. Accelerated molecular dynamics with the bond-boost method. J. Chem. Phys. 119 (12), 6210–6216.
Olsen, R. A., 2006. An introduction to transition state theory. Winter school lecture at Han-sur-Lesse, Belgium.
Perdew, J.P., Burke, K., Ernzerhof, M., 1996. Generalized gradient approximation made simple. Phys. Rev. Lett. 77 (18), 3865.
Qian, X., Liu, J., Fu, L., Li, J., 2014. Quantum spin hall effect in two-dimensional transition metal dichalcogenides. Science 346 (6215), 1344–1347.
Ribas-Arino, J., Shiga, M., Marx, D., 2009. Understanding covalent mechanochemistry. Angew. Chem. Int. Ed. 48 (23), 4190–4193.
Ribas-Arino, J., Shiga, M., Marx, D., 2009. Unravelling the mechanism of force-induced ring-opening of benzocyclobutenes. Chem.–A Eur. J. 15 (48), 13331–13335.
Sheppard, D., Terrell, R., Henkelman, G., 2008. Optimization methods for finding minimum energy paths. J. Chem. Phys. 128 (13), 134106.
Sheppard, D., Xiao, P., Chemelewski, W., Johnson, D.D., Henkelman, G., 2012. A generalized solid-state nudged elastic band method. J. Chem. Phys. 136 (7), 74103.
Song, S., Keum, D.H., Cho, S., Perello, D., Kim, Y., Lee, Y.H., 2016. Room temperature semiconductor-metal transition of $MoTe_2$ thin films engineered by strain. Nano Lett. 16 (1), 188–193.
Tadmor, E.B., Miller, R.E., 2011. Modeling Materials: Continuum, Atomistic and Multiscale Techniques. Cambridge University Press.
Voter, A.F., 1997. Hyperdynamics: accelerated molecular dynamics of infrequent events. Phys. Rev. Lett. 78 (20), 3908.
Wang, Q., Rogers, E.T., Gholipour, B., Wang, C.-M., Yuan, G., Teng, J., Zheludev, N.I., 2016. Optically reconfigurable metasurfaces and photonic devices based on phase change materials. Nat. Photon. 10 (1), 60.
Wang, Y., Xiao, J., Zhu, H., Li, Y., Alsaid, Y., Fong, K.Y., Zhou, Y., Wang, S., Shi, W., Wang, Y., Zettl, A., Reed, E.J., Zhang, X., 2017. Structural phase transition in monolayer $MoTe_2$ driven by electrostatic doping. Nature 550 (7677), 487–491.
Wippermann, S., He, Y., Vörös, M., Galli, G., 2016. Novel silicon phases and nanostructures for solar energy conversion. Appl. Phys. Rev. 3 (4), 40807.
Wuttig, M., Yamada, N., 2007. Phase-change materials for rewriteable data storage. Nat. Mater. 6 (11), 824.
Xu, L., Henkelman, G., 2008. Adaptive kinetic monte carlo for first-principles accelerated dynamics. J. Chem. Phys. 129 (11), 114104.
Zhu, T., Li, J., Lin, X., Yip, S., 2005. Stress-dependent molecular pathways of silica-water reaction. J. Mech. Phys. Solids 53 (7), 1597–1623.